Publications of the Astronomical Society of Australia

*An international journal of
astronomy and astrophysics*

www.publish.csiro.au/journals/pasa

Science with NIFS, Australia's First Gemini Instrument

Peter J. McGregor[1], Michael Dopita[1], Peter Wood[1] and Michael G. Burton[2]

[1]Research School of Astronomy and Astrophysics, Institute of Advanced Studies,
The Australian National University, Canberra, ACT 0200, Australia
peter, mad, wood@mso.anu.edu.au
[2]School of Physics, University of NSW, 2052, Australia
mgb@newt.phys.unsw.edu.au

Abstract: The Near-infrared Integral Field Spectrograph (NIFS) will be Australia's first Gemini instrument. NIFS is a near-infrared, imaging spectrograph that will be used with the ALTAIR facility adaptive optics system on Gemini North to perform near-diffraction-limited imaging spectroscopy over a $3 \cdot 0'' \times 3 \cdot 0''$ field of view with $0 \cdot 1''$ wide slitlets and a spectral resolving power of $\sim$5300. NIFS will operate in the wavelength range from $0 \cdot 94$–$2 \cdot 50\,\mu$m where ALTAIR delivers its greatest gains. Its primary purpose is to study moderate-surface-brightness structures around discrete objects that are revealed at high spatial resolution by ALTAIR. NIFS will address a wide range of science from studies of Galactic star formation and the Galactic centre to the nature of disk galaxies at $z \sim 1$. Studies of the demographics of massive black holes in galactic nuclei and studies of the excitation conditions in the inner narrow-line regions of Seyfert galaxies have been identified as two core NIFS programs. These and other science drivers for NIFS are discussed.

Keywords: instrumentation: spectrographs — galaxies: nuclei — galaxies: Seyfert — infrared: galaxies

1 Introduction

The Research School of Astronomy and Astrophysics (RSAA) of the Australian National University (ANU) has successfully completed the Conceptual Design Review of the Gemini Near-infrared Integral Field Spectrograph (NIFS[1]) and is about to sign a contract with the International Gemini Project Office (IGPO) for the further design, construction and commissioning of the instrument. A preliminary design for NIFS was described by McGregor et al. (1999). NIFS will perform near-diffraction-limited, near-infrared, imaging spectroscopy with the ALTAIR[2] facility adaptive optics (AO) system on Gemini North. It will have a $3 \cdot 0'' \times 3 \cdot 0''$ field of view and divide this field into 29 slitlets, each $0 \cdot 1''$ wide with $0 \cdot 04''$ pixels in the spatial direction. The reformatted slit images will be dispersed with a two-pixel spectral resolving power of $R \sim 5300$ ($\Delta v \sim 60\,\mathrm{km\,s^{-1}}$) in each of the J, H, and K photometric passbands. NIFS is a fast-tracked instrument which will use duplicates of the Near-InfraRed Imager (NIRI[3]) cryostat, On-Instrument Wavefront Sensor (OIWFS), mechanism and temperature control systems, and EPICS control software. The initial detector will be a 2048×2048 HgCdTe HAWAII-2 PACE technology array manufactured by the Rockwell Science Center. The detector system will be developed in collaboration with the Institute for Astronomy of the University of Hawaii.

NIFS science is adaptive optics science. Consequently, much of the Gemini core science that has been described in the science case for ALTAIR will be realised using NIFS in combination with ALTAIR. NIFS is a fast-tracked, limited-capability spectrograph and so will not reproduce all of the Gemini Near-InfraRed Spectrograph (GNIRS) capabilities. The key features of NIFS are its high-spatial-resolution integral field unit (IFU) and its moderate spectral resolution in the 1–$2 \cdot 5\,\mu$m wavelength range; imaging spectroscopy at the maximum spatial resolution attainable with Gemini will be the primary role of NIFS. The application of this technique to the study of the demographics of massive black holes in nearby galactic nuclei, and the related study of the excitation and dynamics of the inner narrow-line regions of nearby Seyfert galaxies, were defined to be NIFS core science (McGregor et al. 1999). NIFS will excel in observations requiring moderate-spectral-resolution data of spatially complex regions having high surface brightness in either a spatial or a spectral sense; spectroscopy of compact, high-surface-brightness continuum sources and imaging of extended, narrow-emission-line regions are examples of these two extremes. These themes feature strongly in the broader science programs described below.

The science capabilities of NIFS cannot be considered in isolation from the requirements imposed by ALTAIR. Consequently, ALTAIR natural guide star requirements are estimated where possible.

2 NIFS Performance

The expected performance of NIFS has been modelled in order to make a realistic assessment of the scientific capabilities of the instrument. The noise sources considered include read noise, dark current noise, cryostat thermal emission, thermal emission from the cryostat window, thermal emission from ALTAIR, thermal emission from

---

[1] http://www.mso.anu.edu.anu/nifs
[2] http://gemini.hia.nrc.ca/altair/
[3] http://kupono.ifa.hawaii.edu/WEB/NIRI/NIRI1.html

Table 1.   Extended, emission line sensitivities (10σ, 1800 s, 100 km s^{-1})

Z grating ($R = 5090$)		J grating ($R = 6100$)	
μ_Z (mag arcsec^{-2})	Σ_{line} (W cm^{-2} arcsec^{-2})	μ_J (mag arcsec^{-2})	Σ_{line} (W cm^{-2} arcsec^{-2})
9·0	$1·6 \times 10^{-21}$	9·0	$1·3 \times 10^{-21}$
10·0	$1·1 \times 10^{-21}$	10·0	$8·4 \times 10^{-22}$
11·0	$7·0 \times 10^{-22}$	11·0	$5·5 \times 10^{-22}$
12·0	$4·5 \times 10^{-22}$	12·0	$3·5 \times 10^{-22}$
13·0	$2·9 \times 10^{-22}$	13·0	$2·3 \times 10^{-22}$
14·0	$2·1 \times 10^{-22}$	14·0	$1·6 \times 10^{-22}$
15·0	$1·4 \times 10^{-22}$	15·0	$1·3 \times 10^{-22}$
16·0	$1·2 \times 10^{-22}$	16·0	$1·0 \times 10^{-22}$
H grating ($R = 5340$)		K grating ($R = 5340$)	
μ_H (mag arcsec^{-2})	Σ_{line} (W cm^{-2} arcsec^{-2})	μ_K (mag arcsec^{-2})	Σ_{line} (W cm^{-2} arcsec^{-2})
9·0	$8·3 \times 10^{-22}$	9·0	$4·9 \times 10^{-22}$
10·0	$5·1 \times 10^{-22}$	10·0	$3·3 \times 10^{-22}$
11·0	$3·2 \times 10^{-22}$	11·0	$2·2 \times 10^{-22}$
12·0	$2·1 \times 10^{-22}$	12·0	$1·8 \times 10^{-22}$
13·0	$1·3 \times 10^{-22}$	13·0	$1·4 \times 10^{-22}$
14·0	$9·5 \times 10^{-23}$	14·0	$1·3 \times 10^{-22}$
15·0	$7·4 \times 10^{-23}$	15·0	$1·2 \times 10^{-22}$
16·0	$6·8 \times 10^{-23}$	—	—

the telescope mirrors, airglow line emission, airglow continuum emission, thermal emission from the sky, and scattered light within the cryostat. Signal photocurrents from point sources were modelled using a point-spread function consisting of a diffraction-limited core and a seeing-limited halo modelled using a Moffat function with index of 11/6 (Racine et al. 1999). This point-spread function is appropriate for partial AO correction. The details of these full simulations are described elsewhere[4]. A simpler, web-based performance calculator is also available[5] and returns similar results for point sources.

These simulations predict that NIFS will be limited by read noise and dark current noise in the J and H bands between strong OH airglow emission lines and by thermal emission from ALTAIR in the K band. NIFS should achieve signal-to-noise ratios of $\sim$10 per spectral pixel in a $0·1'' \times 0·1''$ aperture with median seeing and the expected Strehl ratios of 0·2 at J, 0·4 at H, and 0·6 at K in a single 1800 s on-source exposure on point sources with $Z = 18·8$, $J = 18·4$, $H = 18·8$, and $K = 17·8$ mag in the respective spectral bands. It is assumed that sky subtraction will be achieved using an off-source exposure of the same duration. However, it may be possible in practice to extract sky spectra for uncomplicated fields from field positions within the on-source exposure. NIFS should achieve signal-to-noise ratios of $\sim$10 per spectral pixel in a $0·1'' \times 0·1''$ aperture for single 1800 s on-source exposures on uniform, extended, continuum sources with

surface brightnesses of $Z = 15·4$, $J = 15·0$, $H = 14·8$, and $K = 13·5$ mag arcsec^{-2} in the respective spectral bands. Sky subtraction is again assumed to require an additional off-source exposure of the same duration. The sensitivity to extended line emission depends on both the line width and the background continuum surface brightness. The signal-to-noise ratio achieved in a $0·1'' \times 0·1''$ aperture on extended line emission can be estimated from the above results by comparing the emission-line flux to the noise in the background continuum. The emission-line surface brightnesses, Σ_{line}, required to achieve a signal-to-noise ratio of $\sim$10 per spectral pixel on an extended emission-line source with FWHM = 100 km s^{-1} in a $0·1'' \times 0·1''$ aperture and 1800 s on-source integration time are listed in Table 1 for different background continuum surface brightnesses, μ_λ. Such a spectrum would be suitable for measuring the profile of a 100 km s^{-1}-wide emission line at the full velocity resolution available with each grating. The sensitivities in Table 1 assume that an additional 1800 s off-source exposure is used for sky subtraction. However, sky subtraction may not be necessary when working between strong OH airglow lines in the J and H bands, where little sky emission is expected at the wavelengths of interest.

3 Guide Star Requirements

Observations with NIFS and the ALTAIR natural guide star system will require an optical AO guide star brighter than $R \sim 15$ mag within $\sim$20$''$ of the science object and a near-infrared OIWFS guide star within the 120$''$ diameter

ALTAIR field and brighter than perhaps $K \sim 17$ mag for slow flexure correction. When the ALTAIR laser guide star upgrade has been implemented, an AO guide star with $R < 17$–19 mag and within $\sim 30''$ of the science object (Ellerbroek & Tyler 1998) will still be required for rapid tip-tilt correction. A near-infrared OIWFS guide star will also be required for slow flexure correction, or suitably bright OIWFS guide stars may be used for rapid tip-tilt correction in the near infrared. These are demanding requirements for many science programs.

4 NIFS Core Science

4.1 Massive Black Holes in Nearby Galactic Nuclei

One of the most profound results from the Hubble Space Telescope (HST) is the evidence for the existence of massive (10^7 to $10^9\, M_\odot$) black holes in the nuclei of many nearby early-type galaxies (e.g. Kormendy & Richstone 1995; Lauer et al. 1995; Faber et al. 1997). A relationship appears to exist between the black hole mass and bulge mass, which suggests that either central black holes grew by accreting inner bulge stars, or else that the central black hole and the bulge formed coevally in major merger events. However, this correlation suffers from strong observational selection effects (Ford et al. 1998), and it is yet to be determined whether elliptical galaxies and spiral galaxies follow the same or different correlations. Given the potential close link between black hole formation and galaxy evolution, it is important to define the mass distribution and frequency of occurrence of central black holes in both classes of galaxies. These are still poorly known, most particularly in late-type spiral galaxies in which the nuclear regions are obscured by dust and the bulge masses are smaller so the black hole masses may also be smaller.

Observations with NIFS will help determine the demographics of massive black holes in galactic nuclei. Spatially resolved high-resolution dynamical studies of the innermost nuclear stellar populations and LINER-like gaseous accretion disks at near-infrared wavelengths are necessary to do this. Observations of surface brightness distributions, mean rotation, and radial velocity dispersion profiles with spatial resolutions of a few parsecs and spectral resolutions of 3000–5000 are required to model the stellar dynamics or gaseous accretion disk dynamics and infer properties of the central black hole. The high spatial resolution required dictates the use of AO correction. This and the presence of obscuring dust in the central regions of many galaxies, which complicate the interpretation of optical data from HST, dictate the use of near-infrared observations. The CO (2–0) absorption bandhead at $2\cdot3\,\mu$m is ideal for measuring velocity dispersions of cool stellar populations in the nuclei of low-redshift galaxies (e.g. Gaffney, Lester & Doppmann 1995; Shier, Rieke & Rieke 1996; Böker, van der Marel & Vacca 1999). The presence of a mass concentration is indicated by a rising stellar velocity dispersion profile near the nucleus. The emission lines of H I Pβ $1\cdot282\,\mu$m, H I Brγ $2\cdot166\,\mu$m, [Fe II] $1\cdot257\,\mu$m, and [Fe II] $1\cdot644\,\mu$m

are expected from shock-excited gas in circumnuclear LINER-like accretion disks. The enclosed mass is inferred from the rotational velocity, assuming that the gas follows Keplerian orbits about the mass concentration.

The velocity dispersion profile of M32 rises from $\sigma_V \sim 60\,$km s^{-1} at $1\cdot0''$ radius to $\sigma_V \sim 95\,$km s^{-1} at $0\cdot1''$ radius (Bender, Kormendy & Dehnen 1996). Stellar velocity dispersions are therefore expected to be $\sim 50\,$km s^{-1} in the outer parts and $\sim 100\,$km s^{-1} at the centres of galaxies containing low-mass black holes. These velocity dispersions correspond to Gaussian FWHMs of $\sim 118\,$km s^{-1} and $\sim 235\,$km s^{-1} respectively. A FWHM velocity resolution of $\sim 100\,$km s^{-1} will therefore suffice to measure stellar velocity dispersions from the CO (2–0) absorption bandheads in the K band. The LINER gas disk in the elliptical galaxy M84 has peak rotational velocities of $\pm 400\,$km s^{-1} (Bower et al. 1998), and the gas disk in NGC 4261 has peak rotational velocities of $\pm 200\,$km s^{-1} (Ferrarese, Ford & Jaffe 1996). A velocity resolution of $<100\,$km s^{-1} will be required to measure disk rotational velocities in a range of lower-mass objects. Similarly, high spectral resolving powers of $R \sim 4000$–5000 are required to significantly separate individual OH airglow lines in the J and H bands, in order to perform sensitive measurements of the emission lines from circumnuclear LINER-like disks.

High Strehl ratios are required for these observations. Galaxy nuclei are in general too faint and diffuse to be efficiently used as guide objects for ALTAIR. The laser guide star upgrade to ALTAIR will be required for observations of these objects. A natural guide star within $\sim 30''$ of the nucleus is still required for tip-tilt correction. The required brightness of this star will depend on observing conditions. However, the limiting magnitude in median conditions is expected to be $R \sim 18$ mag (Section 3). Approximately 30 galaxies closer than 20 Mpc, north of declination $-30°$, and having central K-band surface brightnesses $\mu_K < 14\cdot0$ mag arcsec^{-2} at $1''$ resolution have been identified with suitable guide stars. This sample of mainly S0 galaxies will form the initial target list. It will be necessary to accurately determine the point-spread function (PSF) by frequent measurements of a nearby PSF star, by reconstructing the PSF from OIWFS frames, or by modelling based on the AO control loop output (Véran et al. 1997).

It is expected that integration times of several hours will be required to detect massive black holes from stellar velocity dispersions in spiral galaxies closer than ~ 20 Mpc. Figure 1 shows a simulated 3600 s K grating exposure on the nucleus of a spiral galaxy modelled using the light distribution of the Galactic centre. The model galaxy has been shifted to 10 Mpc and no interstellar extinction has been applied. The peak K-band surface brightness in the central $0\cdot1'' \times 0\cdot1''$ region is $\sim 10\cdot5$ mag arcsec^{-2} and is $\sim 12\cdot8$ mag arcsec^{-2} at a fiducial radius of $1\cdot0''$ (~ 50 pc at 10 Mpc). Figure 2 shows the spectrum extracted from the central $0\cdot1'' \times 0\cdot1''$ region after subtraction of a 3600 s sky exposure, transformation for 2D wavelength calibration, and division
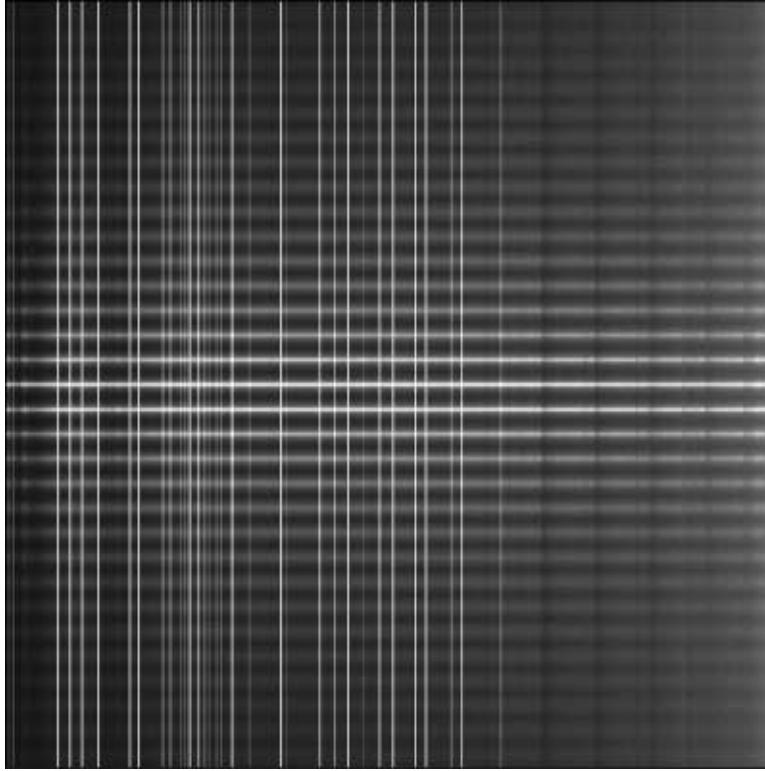
Figure 1 Simulated 3600 s *K* grating exposure of the nucleus of a spiral galaxy at 10 Mpc in 0·4″ seeing with a Strehl ratio of 0·6. Each NIFS slitlet is stacked vertically and dispersed horizontally, with wavelength increasing from ∼2·0 μm to ∼2·4 μm towards the right. The CO $\Delta v = 2$ absorption bands in the galaxy spectrum are apparent at right. The vertical lines are sky emission lines.
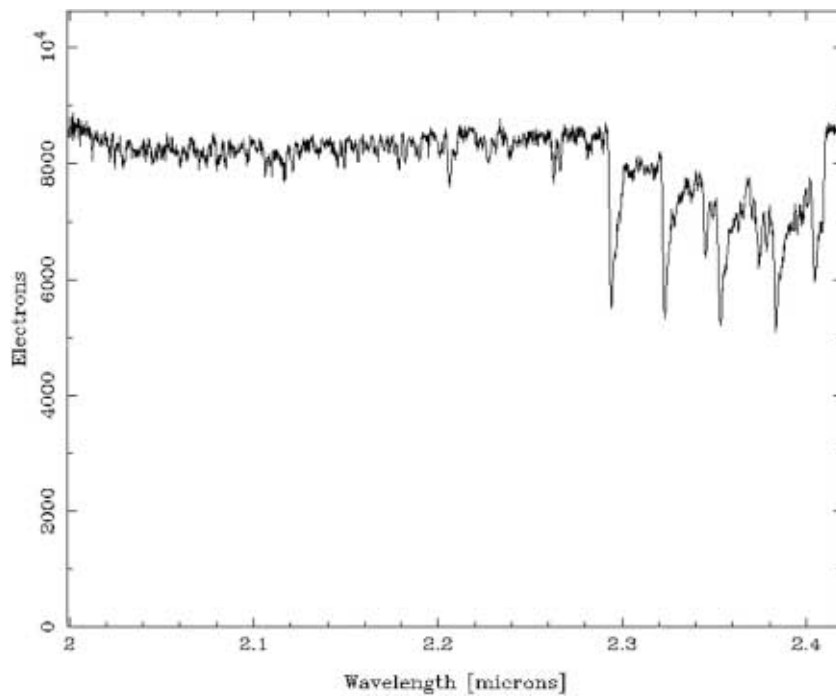

Figure 2 Extracted, sky-subtracted spectrum of the central $0·1″ \times 0·1″$ region of the simulated observation of a spiral galaxy at 10 Mpc shown in Figure 1.

by a smooth-spectrum star. The simulated spectrum has a signal-to-noise ratio of $\sim$100 in this central region (excluding systematic effects due to incomplete sky subtraction and correction for terrestrial atmospheric absorption). Continuum signal-to-noise ratios of $\sim$30 are generally required to measure stellar velocity dispersions for dynamical studies (Kormendy, priv. commun.). When the model galaxy is shifted to 20 Mpc, the K-band surface brightness (with no extinction) at the fiducial radius of $1''$ ($\sim$100 pc at 20 Mpc) is $\sim$13$\cdot$4 mag arcsec^{-2}. A signal-to-noise ratio of 30 is expected to be reached in $\sim$4$\cdot$5 hr of on-source integration with NIFS at this surface brightness (Section 2).

Measurements of black hole masses in nearby galaxies will be limited by spatial resolution as much as by signal-to-noise ratio. The enclosed mass at any radius is derived from the measured stellar velocity dispersion profile and the light distribution using the collisionless Boltzmann equation. Under the reasonable assumptions that the velocity dispersion is approximately constant in the inner region of the galaxy and that the volume mass density is approximately proportional to r^{-2}, the mass enclosed within radius r is given very approximately by

$$M_{\mathrm{enc}} \approx 3 \times 10^7 \left[\frac{r}{0\cdot5''} \right] \left[\frac{D}{10\,\mathrm{Mpc}} \right] \left[\frac{\sigma}{50\,\mathrm{km/s}} \right]^2, \quad (1)$$

where D is the distance to the galaxy, σ is the constant velocity dispersion, and M_{enc} is in units of M$_\odot$. Our model galaxy at 10 Mpc has a velocity dispersion of $\sim$70 km s^{-1} at $0\cdot1''$ ($\sim$5 pc) so an enclosed mass of $\sim$1$\cdot$2 $\times$ 10^7 M$_\odot$ would be inferred. However, our ability to discern the presence of a significant *dark* enclosed mass will depend on the derived value of the enclosed mass-to-light ratio, M_{enc}/L_K. Normal stellar populations can have M_{enc}/L_K in the range 0$\cdot$0–2$\cdot$5 (e.g. Thatte et al. 1997), so we will require mass-to-light ratios in excess of a least 5$\cdot$0 to unambiguously indicate the presence of a massive black hole. Based on the light distribution of the Galactic centre, observations with a resolution of $\sim$0$\cdot$1$''$ will therefore be sensitive to dark enclosed masses $\geq$ 2 $\times$ 10^8 M$_\odot$ at a distance of 10 Mpc. This is comparable to the limit reached by HST with similar spatial sampling.

4.2 Nearby Active Galactic Nuclei

Many nearby galaxies possess active galactic nuclei which are characterised by broad (FWHM $\sim$ 500 km s^{-1}) emission lines originating in their central regions over size scales of 100 pc up to $\sim$2 kpc. This is the so-called narrow-line region (NLR). The ultimate energy source is believed to be accretion onto a massive black hole in most objects, although intense starbursts in dense regions may be responsible for some LINER-like activity (Terlevich & Melnick 1985). Emission from the immediate vicinity of the accretion disk produces the broad-line region (BLR), which remains unresolved with existing telescopes. Understanding the nature of the central energy source, its interaction with the host galaxy, and

the global implications for the evolution of galaxies are continuing themes in the study of active galactic nuclei (AGN). High-spatial-resolution optical studies of AGN with HST (e.g. Capetti et al. 1996; Winge et al. 1997; Axon et al. 1998) have revealed a wealth of information about the structure and excitation of the inner NLR. While it has traditionally been believed that the NLR clouds are photoionised by the central source (Ferland & Netzer 1983; Wilson & Tsvetanov 1994), these recent high-spatial-resolution imaging and dynamical studies have demonstrated that NLR clouds may instead be predominantly shock-excited by energetic thermal and non-thermal mass outflows from the central object. Strong dynamical interaction between the emission-line gas and radio-emitting ejecta can be explained if the NLR is formed from shells of ambient interstellar medium swept up and compressed by the supersonic expansion of hot gas heated by interactions with the advancing radio jet (Pedlar, Unger & Dyson 1985; Taylor, Dyson & Axon 1992; Steffen et al. 1997). The nuclear regions of Seyfert galaxies are invariably obscured by dust clouds, making near-infrared observations of the inner NLR desirable. The near-infrared region also offers the best ground-based spatial resolution using AO correction. [Fe II] 1$\cdot$257 μm, [Fe II] 1$\cdot$644 μm, H I Pβ 1$\cdot$282 μm, and H I Brγ 2$\cdot$166 μm emission lines are well-suited to excitation and dynamical studies of the high-excitation precursor zones associated with fully radiative shocked regions. Strong coronal emission lines are the primary initial coolants of hot gas in partially radiative shocks. With NIFS, the [Si VI] 1$\cdot$961 μm coronal line will become accessible at modest redshift. The mechanical energy flux from the jet can be estimated from the [Fe II] and H I Pβ lines in less obscured regions, and from H I Brγ in more obscured regions. H$_2$ 1–0 S(1) 2$\cdot$122 μm emission in Seyfert galaxies is also collisionally excited, but generally has a smaller velocity width of $\sim$300 km s^{-1}, suggesting that it may arise in a different emission region (Veilleux, Goodrich & Hill 1997). X-ray heating from the AGN core, shock heating by the interaction of the radio jets with the interstellar medium, and shock excitation in outflows from star formation regions may all contribute to the H$_2$ emission from Seyfert galaxies. High-spatial-resolution dynamical studies may provide a means of distinguishing between these alternatives.

Seyfert activity is frequently associated with circumnuclear starbursts, often in rings, but the role these play in fuelling or refuelling the active nucleus is still unclear. The presence of circumnuclear starburst rings demonstrates that large quantities of gas have been channelled into the region close to the nucleus. This gas may accrete directly onto the black hole, but it must lose its remaining angular momentum to do this. It may be the stars, or their remnants, formed in the starburst ring or the central star cluster that feed the central black hole. High-angular-resolution spectral imaging of Seyfert galaxy cores will reveal structure interior to the starburst ring. The morphology and dynamics of the emission-line regions will permit new

insight into how gas is funnelled into the core, and the role possibly played by stellar bars in driving such gas flows. Measurement of stellar mass-to-light ratios, M/L_K, will probe the star formation histories of the regions. Detailed comparison of spatially resolved spectra with starburst models (e.g. Leitherer et al. 1999) will provide estimates of the starburst ages, masses and star formation histories. These can then be compared to particular models for AGN fuelling (e.g. Norman & Scoville 1988). The potential of AO-corrected imaging of Seyfert galaxy cores in addressing these issues is beginning to be explored (Marco, Alloin & Beuzit 1997; Chapman, Walker & Morris 1999; Rouan et al. 1998; Marco & Alloin 1998, 2000).

Measurement of the central black hole masses in Seyfert galaxies is also highly desirable. Although these can be estimated using reverberation-mapping techniques for a few objects (e.g. Wandel, Peterson & Malkan 1999), stellar velocity dispersions provide a more direct determination. Stellar velocity dispersions can be measured using the CO (2–0) absorption bandheads, and interpreted in the same way as for normal galaxies (Section 4.1) to place limits on the enclosed mass, and hence detect or constrain black hole masses. The analysis is complicated in the case of common Seyfert galaxies by the intense Seyfert core emission. Minimising this contamination will depend on achieving high Strehl ratios in the telescope, ALTAIR and NIFS. However, approximately 43% of nearby galaxies show a detectable level of nuclear activity (Ho, Filippenko & Sargent 1997). These galaxies may contain either lower-mass black holes or massive black holes that are currently accreting at well below their Eddington limits. These galaxies will be prime candidates for observation with NIFS. The core of the nearest Seyfert galaxy, Circinus, has a radius of <1·5 pc at K (Maiolino et al. 1998), corresponding to <0·08″. The stellar velocity dispersion within ∼40 pc (∼2″) of the nucleus is ∼75 km s^{-1}, corresponding to a Gaussian FWHM of ∼180 km s^{-1}. We require a velocity resolution of ∼100 km s^{-1} to confidently measure such velocity dispersions.

The AO requirements on Seyfert galaxy programs are less severe than for normal galaxies. Many Seyfert nuclei are bright enough and sufficiently compact to be used as ALTAIR guide stars. A large number of nearby Seyfert galaxies in the Shapley–Ames catalogue were checked for nearby stars. Approximately 20% have suitably bright guide stars within ∼30″ of the nucleus. High Strehl ratios are needed to measure black hole masses, and are desirable when studying emission from NLR clouds.

5 Gemini Core Science

5.1 Brown Dwarfs and Low-mass Stars

Recent near-infrared sky surveys have succeeded in identifying large numbers of low-mass stars and brown dwarfs. However, objects in binary systems still offer the only means of empirically determining precise masses and absolute magnitudes for this class of object. These data are basic to an understanding of the low-mass stellar and substellar mass function, and ultimately the transfer of angular momentum during star formation and the universal proportion of matter bound up in sub-stellar companions. The distances to objects in binary systems can be determined, so they provide empirical calibration of the colour versus absolute magnitude relation that can be applied to field and cluster brown dwarf candidates. NIFS with occulting disks will record moderate-resolution near-infrared spectra of the close companions that will provide effective temperatures and other physical parameters for the companions. The imaging capability of NIFS will be invaluable in removing the complex residual 'speckle' pattern of the bright primary star.

Spectra in the J, H and K bands with a resolving power of $R \sim 1000$ are sufficient to determine molecular absorption band strengths for temperature determination (e.g. Gl229B, $K \sim 14·8$ mag; Geballe et al. 1996). The central star can be used as the ALTAIR guide star in all conceivable cases. Finding a nearby OIWFS guide star will be subject to random field statistics.

The performance of NIFS in detecting binary companions has been assessed by determining the signal-to-noise ratio that will be achieved in spectra obtained with the K grating and smoothed to a two-pixel resolving power of $R \sim 1000$. The image obtained from a simulated NIFS observation of a $K = 12$ mag primary and $K = 18$ mag secondary by collapsing the data in the spectral direction is shown in Figure 3. The $R = 1000$ sky-subtracted spectrum of the secondary star is shown in Figure 4 (ignoring PSF uncertainties and residual speckle structure in the primary star profile). These simulations predict that NIFS will saturate using the K grating in 1800 s on a $K \sim 12$ mag primary star in 0·4″ seeing with a Strehl ratio of 0·6. A signal-to-noise ratio of ∼18 will be achieved in the $R = 1000$ spectrum of a 0·5″ offset companion star with $K = 18$ mag in this time. Integration times will be limited to 15 s on a $K = 7$ mag primary star. The signal-to-noise ratio achieved on an 18 mag secondary in a total integration time of 1800 s is then ∼4.

5.2 Young Star Clusters

A knowledge of the stellar initial mass function over the full range of masses from the Eddington limit to below the hydrogen-burning limit, and its dependence on environment, is fundamental to an understanding of the star formation process. The upper stellar mass cutoff needs to be explored in nearby regions of massive star formation in order to better understand the nature of massive star formation occurring in more extreme regions such as starburst galaxies. Concentrations of high-mass stars are found in young Galactic star clusters. These are often obscured by dust due to their youth or their large distances from Earth. High-spatial-resolution observations are needed to probe the cores of dense star clusters associated with Galactic giant H II regions (e.g. Blum, Damineli & Conti 1999) and clusters in the vicinity of the Galactic centre (e.g. Cotera
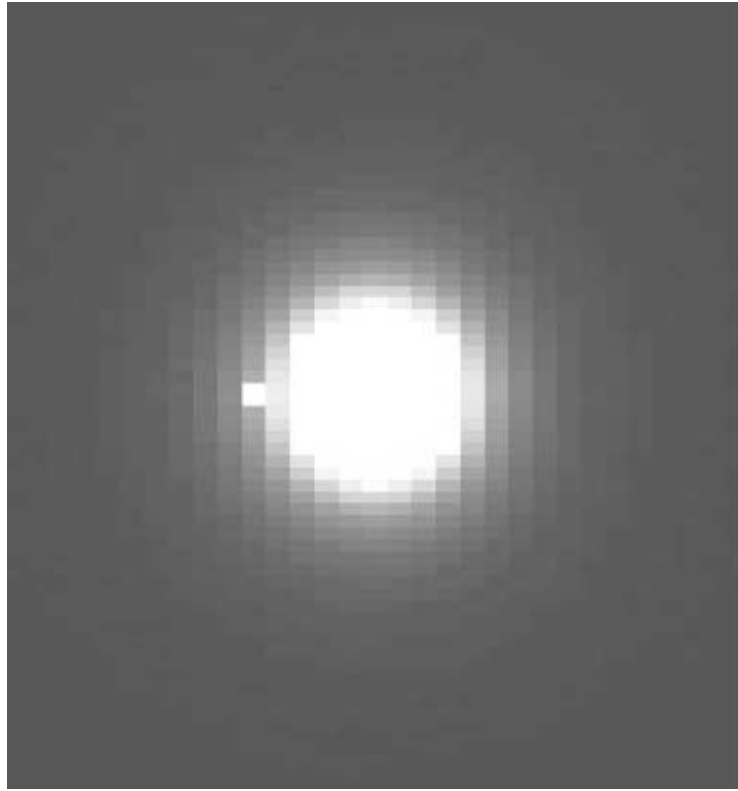
Figure 3   Simulated collapsed NIFS image showing a $K = 18$ mag companion star $0 \cdot 5''$ to the left of a $K = 12$ mag primary star in $0 \cdot 4''$ seeing with a Strehl ratio of $0 \cdot 6$. The exposure time with the K grating is 1800 s, which just saturates the $K = 12$ mag star.
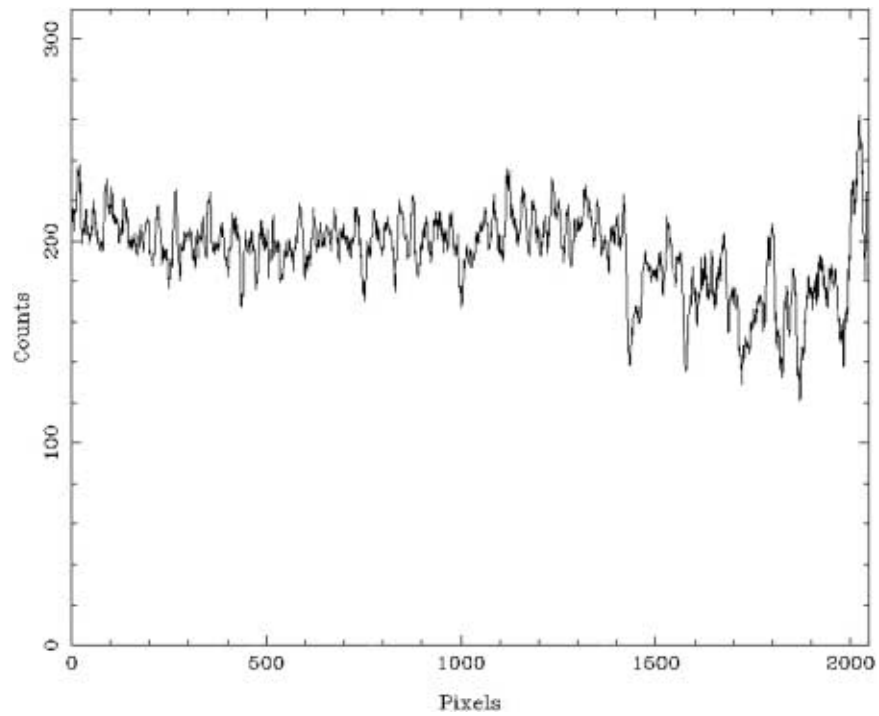

Figure 4   Spectrum of the $K = 18$ mag M1III star companion in Figure 3, smoothed to a two-pixel resolving power of $R = 1000$. Atmospheric absorption features have been removed by division by a smooth-spectrum star.

et al. 1996). The physical parameters of embedded massive stars can be derived from high signal-to-noise ratio ($\sim$70), moderate-resolution ($R > 1000$) spectra in the H and K bands (Blum, Damineli & Conti 1999; Hanson, Howarth & Conti 1997; Hanson, Conti & Rieke 1996).

Knowledge of the low-mass end of the stellar initial mass function in different environments is needed to determine the amount of Galactic mass locked up in low-mass stars, to understand chemical enrichment and recycling in galaxies, and to determine the impact of starbursts on galaxy evolution. Most low-mass stars currently forming in the Galaxy appear to be forming in star clusters associated with giant molecular clouds (Lada et al. 1991). Stellar masses for lower-mass pre-main-sequence stars ($M < 5M_\odot$) cannot be determined unambiguously from broadband near-infrared photometry alone, due to the indeterminate effects of interstellar extinction and the nature of their evolutionary tracks. Moderate-resolution K band spectra of these obscured, low-mass, cluster pre-main-sequence stars are required to assign them spectroscopic temperatures (Hodapp & Deane 1993; Luhman & Rieke 1998), and hence infer their masses based on evolutionary tracks.

Source confusion and the irregular backgrounds from complex reflection and emission nebulosity associated with dense young star clusters make slit spectroscopy of faint, embedded, young stars difficult. NIFS, with its IFU, will allow more accurate removal of these irregular backgrounds. The compact W43 cluster (Blum, Damineli & Conti 1999) contains stars measured photometrically to $K \sim 16$ mag, corresponding to a spectral type of $\sim$A0 on the main sequence. NIFS will be capable of measuring K-band spectra of these stars with $R \sim 5000$ and signal-to-noise ratios of $\sim$40 in 1800 s.

5.3 YSO Jet Driving Mechanism

The driving mechanism for outflows from young stellar objects (YSOs) has not been observationally identified. Shocked, collimated jets are seen at large distances from the star, but the properties of the winds at their origins, and even the mass loss rates, remain uncertain and model-dependent. High-spatial-resolution spectral imaging in emission lines probing shocked gas, such as H_2 1–0 S(1) $2 \cdot 122\,\mu$m and [Fe II] $1 \cdot 644\,\mu$m, will allow observation of the energetic, highly collimated jets as they emerge from the inner regions of the accretion disks. The high spectral resolution of NIFS, relative to narrow-band line filters, will enable better discrimination against continuum emission, making NIFS the preferred Gemini instrument for near-infrared spectral imaging of faint, narrow emission-line sources. High-resolution spectral imaging of YSO jets with NIFS will provide simultaneous morphological, excitation and kinematic data which, over time, will allow the evolution of features in these stellar jets to be traced as they progress along the jet and interact with the surrounding material. Such observations are crucial to understanding the role played by high-energy outflows in terminating infall and determining the final stellar mass. For example, a 'Herbig–Haro' emission knot located in a nearby dark cloud $\sim$150 pc from Earth and moving at 100 km s^{-1} traverses $0 \cdot 13''$ in one year. Proper motions of such Herbig–Haro knots could be followed over a 2–3 yr period, allowing the acceleration mechanism to be probed as well as the interaction of these knots with the ambient cloud. Temporal variations in an extremely young Herbig–Haro flow ejected from XZ Tau have been seen in the optical with HST (Krist et al. 1999). Emission-line spectroscopy of such features with NIFS will reveal details of how the flows expand and evolve.

The targeted emission lines will be the H_2 lines in the K band and [Fe II] $1 \cdot 644\,\mu$m in the H band. The H_2 1–0 S(1) $2 \cdot 122\,\mu$m and H_2 1–0 Q(3) $2 \cdot 424\,\mu$m emission lines arise from the same $J = 3$ upper level so their flux ratio can be used to derive the interstellar extinction correction. This is one motivation for extending the NIFS K grating response to the edge of the atmospheric window near $2 \cdot 5\,\mu$m. These observations require the highest possible spatial and velocity resolutions in the H and K bands of 50–100 km s^{-1}. Velocity centroids can be determined to $\Delta v \sim$ FWHM/SNR, which should be $\sim$5–10 km s^{-1} with typical signal-to-noise ratios. Visible T Tauri stars can be used as natural guide stars for ALTAIR, when available, but a different star will be required for the OIWFS. The near-infrared response of the NIFS OIWFS will greatly increase the availability of suitable OIWFS stars in star formation regions. Many YSOs either are not visible objects or are resolved in the optical. Laser guide stars will be essential for AO-corrected observations of these stars.

5.4 YSO Jet–Cloud Interactions

YSO outflows remove excess angular momentum from the protostar system, they contribute to the turbulent support of molecular clouds, and they may be responsible for disrupting molecular clouds and ultimately terminating star formation within them. YSO outflows generally consist of a highly collimated, high-velocity bipolar jet embedded in a less well collimated, low-velocity bipolar molecular outflow that is detected at millimetre wavelengths. The physical parameters of the highly collimated YSO jets are still incompletely understood. They emit most strongly in shock-excited transitions of H_2 and [Fe II] in the near-infrared, and low-excitation emission lines typical of Herbig–Haro objects in the optical in regions where the jet material impacts the surrounding medium. A bow shock forms where shocked gas impacts quiescent material in front of a Mach disk, which forms where the jet impacts previously shocked material. Observed emission line strengths can be modelled either as J-shocks, C-shocks or a combination of the two (e.g. Buckle, Hatchell & Fuller 1999). J-shocks occur where the magnetic field is weak, and cause the gas properties to change suddenly. C-shocks occur in the presence of a strong magnetic field. A C-shock can form at the bow shock and a J-shock can form at the Mach disk when the magnetic field is intermediate in strength. Which type of shock

applies in YSO jet–cloud interactions is still controversial. The relative emission line strengths give an indication of the type and speed of the shock (Smith 1995). The bow shock and Mach disk are expected to be separated by $\sim$500 AU ($\sim$3·4″ at 150 pc) in most cases (Hartigan 1989), but the curved structure of the bow shock complicates identification of this feature. High-spatial-resolution spectral imaging with NIFS may succeed in separating these components.

YSO jets often have a knotty appearance, possibly due to jet instabilities or episodic ejection. Emission arising from between the knots may be due to the jet being partially molecular, to entrainment of ambient material in a mixing layer, or simply to the existence of unresolved emission knots. YSO jets have many similarities (and differences) with relativistic jets emanating from radio galaxies. Understanding the physical processes occurring in YSO jets may also help in understanding the nature of these extragalactic jets.

Spatially resolved NIFS spectra in the K band are needed to determine H_2 emission line fluxes, flux ratios and radial velocities. Proper motions for knots within the jet are also needed to test jet models quantitatively. Typical jet velocities are $\sim$200 km s^{-1}. Projected velocities are correspondingly lower, so velocity resolutions of $\sim$50 km s^{-1} are required. Optical AO guide stars may be scarce in dark clouds, making laser guide star observations highly beneficial. It will be possible to use nearby embedded stars as the near-infrared OIWFS guide star in many cases.

5.5 Late Stages of Stellar Evolution

In recent years, HST and deep ground-based imaging of asymptotic giant branch (AGB) stars, proto-planetary nebulae and young planetary nebulae have revealed remarkable but previously unknown structures. These show exquisite detail of central, point-symmetric, often bipolar, cavities being carved out of the centres of spherical AGB-star mass-loss envelopes (Sahai et al. 1998; Sahai et al. 1999a,b; Sahai & Trauger 1998). How such non-spherical cavities can be produced inside the recent spherical AGB-star mass-loss wind is an unsolved mystery. Binarity, rotation, and magnetic fields have all been suggested. Most importantly, it is the immediate post-AGB phase where the asymmetries develop, so it is here that we should look for objects beginning the aspherical mass-loss process. Samples of candidate objects are currently being examined from the ground (e.g. van der Steene & Wood 1999, priv. commun.). They often show Hα emission with a central peak of width $\sim$100 km s^{-1}, a P Cygni-type absorption on the blue edge of the emission line, and broad wings with widths of order 1000 km s^{-1}. High spatial and spectral resolution observations of these objects are required in order to examine the gas-dynamical processes occurring in them. In particular, K-band observations in the lines of H_2 1–0 S(1) 2·122 μm and H I Brγ 2·166 μm are required in order to study the beginning of cavity generation (as evidenced by H_2 emission from shocked gas) and

to determine the location of the H II region: is it a wind from the AGB star remnant, is it a jet from an accretion disk around a companion star, do the broad 1000 km s^{-1} and 100 km s^{-1} components of the H I lines come from the same place spatially? Velocity resolutions of a few km s^{-1} are required for this work in order to make models of the gas flows in these systems. Since the H_2 emission has been detected by NICMOS, it should be measurable with NIFS. Many proto-planetary nebulae and most young planetary nebulae have central stars that can be used as guide stars for ALTAIR. OIWFS guide stars will be subject to random field statistics.

5.6 Galactic Centre

The Galactic centre is a unique region of the Galaxy populated by old stars constituting the inner Galactic bulge as well as young clusters of massive stars indicative of recent intense star formation activity. There is now strong evidence for the existence of a central massive black hole in the Galactic centre (Eckart & Genzel 1996, 1997; Genzel et al. 1997; Ghez et al. 1998). High spatial and moderate spectral resolution observations of stars in the vicinity of the black hole are required to determine their radial velocity dispersion, to complement available high-spatial-resolution proper motion data, and to study the nature of the stellar population. Stars close to the black hole should interact with the black hole and with each other frequently, and may show evidence for these interactions in their spectral or morphological properties. Understanding the star formation history of the central region of the Galaxy will lead to a clearer understanding of the formation of the Galactic bulge; the nature of star formation in an environment of extreme gas temperature, pressure, velocity dispersion, magnetic field strength and tidal shear; and of the processes fuelling the central black hole in our Galaxy and perhaps in other more active galaxies.

The Galactic centre is obscured at wavelengths shorter than $\sim$1·5 μm. Most of the bright stars detected in the K band are young late-type supergiant and AGB stars or older luminous red giant stars. Main-sequence stars are intrinsically fainter in the near infrared, and so are more difficult to detect. Nevertheless, main-sequence stars in the volume around the Galactic centre are being found in deep photometric surveys using conventional techniques (e.g. Blum, Sellgren & DePoy 1996) and AO image correction (Davidge et al. 1997b). Near-infrared spectra are needed for significant samples of faint stars in the crowded Galactic centre region in order to estimate effective temperatures, extinctions, luminosities, and hence masses and ages. NIFS will be well-suited to this task (Figure 5); its spectral resolution, spatial resolution, sensitivity and ability to accurately characterise complex background emission are all essential. Techniques for spectrally classifying early-type stars based on high signal-to-noise ratio $R \sim 1000$ H-band and K-band spectra are now in place (e.g. Ali et al. 1995; Blum et al. 1997; Hanson, Rieke & Luhman 1998). Higher spectral resolving powers of $R > 3000$ are required for radial velocity measurements
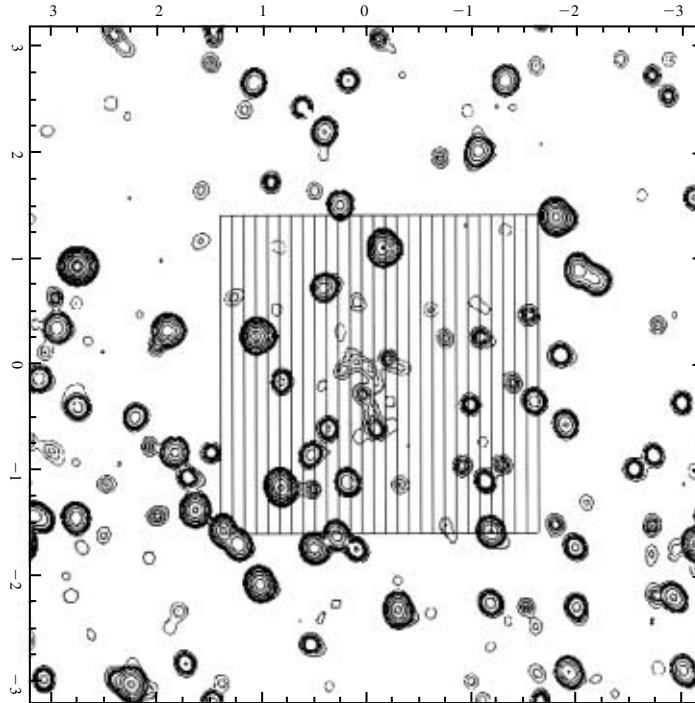
Figure 5 K-band image of the Galactic centre region (Eckart et al. 1995) centred on Sgr A*, the central black hole, with the NIFS field of view (square grid) superposed. The axis units are arcseconds on the sky.

of stars in the immediate vicinity of the central massive black hole. Present AO-corrected imaging (Davidge et al. 1997b) extends to $K \sim 16$ mag. Early-type main-sequence stars are expected at $K > 14$ mag. High signal-to-noise ratio spectra of these stars can be measured with NIFS in ~ 1 hr per field. High Strehl ratios are essential to separate individual stars in this crowded region. A star with $R = 13 \cdot 9$ mag ('star A') is located $18 \cdot 8''$ from Sgr A* and can be used as the AO guide star for observations of the central region. A range of near-infrared-bright OIWFS guide stars exist.

5.7 Nuclear Stellar Populations in Local Group Galaxies

Little is known about the nuclear stellar populations in Local Group galaxies. Near-infrared spectra of nuclear stellar populations obtained with NIFS will provide information on the stellar content and star formation histories of nearby galaxies. The nucleus of M31 is known to be double (Lauer et al. 1993) and to consist of separate red and blue brightness peaks. The massive black hole is believed to reside within the blue peak, P2. This appears to be the nuclear star cluster but its stellar content and star formation history remain unclear. The dynamical state of the red peak, P1, is mysterious. The instability timescale for a star cluster in this environment is $\sim 10^4$ yr indicating that additional stabilising influences must be in play. Tremaine (1995) suggested that the brightness peak at P1 can be explained as the apogalactica of stars orbiting P2 in an eccentric disk. A similar double nucleus is present in another massive black hole galaxy,

NGC 4486B (Lauer et al. 1996), and blue nuclear star clusters similar to P2 occur in the Local Group late-type galaxies M33 (e.g. Kormendy & McClure 1993) and IC 342 (Böker, van der Marel & Vacca 1999). Many parallels exist between these Local Group nuclear star clusters and the Milky Way nuclear star cluster. Infrared spectra in combination with optical and ultraviolet spectra of these blue nuclear star clusters in Local Group galaxies provide insight into the reddening, mass and age of the starbursts that have formed them or recently activated them (e.g. Gordon et al. 1999; Böker et al. 1999).

5.8 Old Stellar Populations in Nearby Galaxies

ALTAIR on Gemini will resolve stars in nearby galaxies and hence make their stellar populations accessible to photometric and spectroscopic study. AGB stars in several nearby galaxies have been studied photometrically in the optical with WFPC2 on HST. These photometric studies have only recently been extended to the near infrared with AO systems on ground-based 4 m telescopes (e.g. the nucleus of M31; Davidge et al. 1997a). Source confusion remains a problem with $0 \cdot 15''$ spatial resolution in the central regions of even nearby galaxies. The smaller, diffraction-limited images from ALTAIR on Gemini will alleviate much of this problem. However, the high Strehl ratios that are required will restrict these observations to the near infrared. At infrared wavelengths, the stellar population is dominated by AGB and red giant branch (RGB) stars. Near-infrared spectra of individual stars will provide information that will lead to a better understanding of the chemical abundances and abundance ranges of

stars in Local Group galaxies. The CO 2–0 absorption bands at $2 \cdot 3 \, \mu m$ are the primary abundance indicator in late-type stars. The $1 \cdot 62 \, \mu m$ feature, due mainly to CO 6–3 absorption, has also been used in late-type stars with [Fe/H] $\geq -1 \cdot 3$ (Origlia et al. 1997).

Studies of AGB stars should reach to $M_K \sim -7 \cdot 0$ mag, or $K \sim 17 \cdot 5$ mag at the distance of M31 and its dwarf elliptical satellite galaxy M32 ($m - M \sim 24 \cdot 5$ mag). These are among the brightest old stars in these galaxies. NIFS with ALTAIR will achieve a signal-to-noise ratio in the K band of ~ 10 per pixel in 1800 s with $R = 5340$ at the AGB tip. Smoothing to $R = 1000$, which is adequate for CO-band studies, will increase the signal-to-noise ratio to ~ 23 per pixel. The central $2 \cdot 8''$ diameter nuclear region of M31 contains ~ 20 objects with $K = 14 \cdot 5$–$16 \cdot 5$ mag detected with AO imaging (Davidge et al. 1997a). These stars are exceptionally bright and are either a separate population of young massive stars (as in our galaxy), or they are unresolved star clusters. The tip of the red giant branch in globular-cluster-like populations similar to 47 Tuc occurs at $M_K \sim -5 \cdot 0$ mag (Frogel, Persson & Cohen 1981), corresponding to $K \sim 19 \cdot 5$ mag at the distance of M31 and M32. K-band observations of these stars at $R = 1000$ will require integration times of $\sim 2 \cdot 5$ hr to reach a signal-to-noise ratio of ~ 10 per pixel. The success of these observations will depend critically on the Strehl ratio achieved; high Strehl ratios increase signal-to-noise ratio and reduce source confusion, which will be severe at these fainter magnitudes. The star count models of Ratnatunga & Bahcall (1985) predict that there will be $\sim 0 \cdot 3$ star arcmin^{-2} with $R < 16 \cdot 5$ mag along the sightline to M31 and M32, assuming a typical $B - R$ color of $0 \cdot 5$, so there should be ~ 1 suitable AO guide star per $2'$ diameter ALTAIR field in this direction. Observations will be restricted to regions within $\sim 15''$ of these AO guide stars. Spatial information obtained with the NIFS IFU will aid accurate background removal.

High signal-to-noise ratio, moderate-resolution spectra are required for detailed chemical abundance studies. At the full resolution available with the K grating, a signal-to-noise ratio of 100 will be obtained in 1 hr on a star with $K \sim 15 \cdot 0$ mag. Thus it will be possible with NIFS to obtain full resolution K-band spectra of RGB-tip stars with $m - M < 20$, or distances < 100 kpc. This will enable detailed chemical abundance analyses of RGB-tip stars in local dwarf galaxies and in the Galactic halo. These spectra will also provide dynamical information.

5.9 Nearby Starburst Galaxies and Starburst Regions

Nearby starburst galaxies are excellent laboratories for studying the dissipation processes that are believed to have occurred when galaxy spheroids formed. The dominant structural components of nearby starburst galaxies have now been spatially resolved in the ultraviolet and optical with HST; WFPC2 images reveal large numbers of 'super star clusters', which resemble young, massive (10^5–$10^6 \, M_\odot$) globular clusters and which have properties more extreme than those of 30 Dor in the Large Magellanic Cloud, for example. Near-infrared ground-based observations (e.g. NGC 1808; Tacconi-Garman, Sternberg & Eckart 1996) identify presumably young super star clusters embedded in dust with $A_V \sim 10$–20 mag. These optically hidden super star clusters may contain the youngest and most massive stars. Studying individual super star clusters spectroscopically in the near infrared will allow starburst models to be applied to specific coeval components of the overall starburst. The distribution of interstellar extinction in starburst regions affects our interpretation of starburst energetics. Measuring extinction indicators on spatial scales comparable to the dominant starburst structures will improve our ability to distinguish between foreground screen and mixed extinction models for these components, leading to more accurate interpretations. Comparison of the ages and star formation rates derived for different locations within the starburst will reveal how the starburst has progressed through the region.

Typical continuum and emission-line surface brightnesses can be estimated from knots in the starburst ring of NGC 7552 (Schinnerer et al. 1997). The K-band continuum surface brightnesses are $K \sim 13 \cdot 0$–$13 \cdot 5$ mag arcsec^{-2}, and the prominent emission-line surface brightnesses are ~ 8–25×10^{-23} W cm^{-2} arcsec^{-2}. Emission lines with surface brightnesses of $\sim 14 \times 10^{-23}$ W cm^{-2} arcsec^{-2} and FWHM ~ 100 km s^{-1} should be measured with NIFS to a signal-to-noise ratio of 10 in 1800 s with $0 \cdot 1'' \times 0 \cdot 1''$ spatial resolution. A mosaic of 3×3 NIFS fields would be needed to fully map the starburst ring and nucleus of NGC 7552.

5.10 Ultra-luminous Infrared Galaxies

Ultra-luminous infrared galaxies (ULIRGs) occur in the late phases of the merger of two or more gas-rich galaxies. They may be the merger remnants of former compact galaxy groups (Borne et al. 2000). They have massive ($\sim 10^{10} \, M_\odot$; Solomon et al. 1997), dense ($n_{H_2} \geq 10^4$ cm^{-3}; Solomon, Downes & Radford 1992) concentrations of molecular gas and dust in their central regions and are powered by either intense, compact starbursts or AGN activity. Their luminosities ($> 10^{12} \, L_\odot$), space density, activity, and short evolutionary timescales ($\sim 10^8$ yr) suggest that they may represent an early phase in the formation of quasars (Sanders et al. 1988). Double nuclei with subarcsecond separations are seen in several well studied examples. These are interpreted as the remnant nuclei of the merged galaxies. Several ULIRGs have K light profiles that are well fitted with a $r^{1/4}$ de Vaucouleurs law, suggesting that elliptical galaxies will be the end result of the mergers (Wright et al. 1990; Doyon et al. 1994) and that their high central mass densities are comparable to those of elliptical galaxies (Kormendy & Sanders 1992); ULIRGs may be analogues of proto-elliptical galaxies formed at high redshift. They are currently undergoing dissipative collapse, which may also be analogous to spheroid formation in disk galaxies.

High-angular-resolution spectral imaging with NIFS will probe the stellar populations and emission-line characteristics on spatial scales commensurate with the nuclear separations. These data will provide information on star formation rates, starburst lifetimes and the nature of the stellar initial mass function close to the compact luminosity sources, as well as information on the gas dynamics in the region where the nuclei interact. Velocity dispersion data can be used to derive mass estimates for the enclosed regions. Both emission-line and stellar absorption-line diagnostics can be used for this purpose. Extending these studies to smaller radii will place tighter constraints on the compact luminosity sources. Millimetre molecular line data with $0.5''$ resolution for Arp 220, for example, suggest that the double nuclei are each surrounded by counter-rotating gas disks with radial extents of $\sim 0.3''$ (Sakamoto et al. 1999). The formation of nuclear gas disks during galaxy mergers may be a natural consequence of the high dissipation rates in dense gas. However, the likely role these disks play in driving nuclear starbursts or fueling AGN activity has yet to be explored. Interaction between these disks should be apparent in near-infrared, shock-excited emission lines such as [Fe II] $1.644\,\mu m$ and various H_2 transitions in the K band. These features will be sampled with NIFS at higher spatial resolution than that currently achieved at millimetre wavelengths. Studies to date show shock-excited emission-line tracers can peak *between* the two nuclei (e.g. NGC 6240; van der Werf et al. 1993), whereas starburst tracers such as H I Brγ emission peak on the nuclei (e.g. Arp 220; Larkin et al. 1995). NIFS will have the spatial and spectral resolution, and the sensitivity, to examine these interactions in detail.

Arp 220 is considered as an example because of the availability of high-spatial-resolution NICMOS data for this object (Scoville et al. 1998). The two nuclei in Arp 220 are separated by $\sim 200\,km\,s^{-1}$ in H I Brγ (Larkin et al. 1995). The Brγ fluxes from the eastern and western components are $\sim 5.3 \times 10^{-23}\,W\,cm^{-2}$ and $\sim 6.5 \times 10^{-23}\,W\,cm^{-2}$ respectively, summed over $200\,km\,s^{-1}$. We assume that the flux from the eastern and western components extend over $0.2'' \times 0.2''$ and $0.5'' \times 0.2''$ respectively, based on NICMOS continuum images (Scoville et al. 1998). The emission-line surface brightnesses are then $\sim 1.3 \times 10^{-21}\,W\,cm^{-2}\,arcsec^{-2}$ and $\sim 6.5 \times 10^{-22}\,W\,cm^{-2}\,arcsec^{-2}$ for the eastern and western components respectively. The continuum surface brightnesses through the same apertures correspond to $K \sim 10.7\,mag\,arcsec^{-2}$ and $\sim 10.5\,mag\,arcsec^{-2}$ respectively. A signal-to-noise ratio of 10 per spectral pixel will be achieved with NIFS in the K band in $1800\,s$ on a $200\,km\,s^{-1}$-wide emission line against a $10.5\,mag\,arcsec^{-2}$ continuum with $0.1'' \times 0.1''$ spatial resolution at an emission-line surface brightness of $5.5 \times 10^{-22}\,W\,cm^{-2}\,arcsec^{-2}$, similar to the expected emission-line surface brightness of the Arp 220 components.

A similar velocity offset is seen in NGC 1614, where the velocity separation of the two nuclei is $\sim 150\,km\,s^{-1}$,

with each component having a velocity dispersion of $\sigma_V \sim 50$–$60\,km\,s^{-1}$ and together having a total Brγ emission-line flux of $\sim 6 \times 10^{-21}\,W\,cm^{-2}$ through a $\sim 2.4'' \times 4''$ aperture (Puxley & Brand 1999). Stellar velocity dispersions in ULIRGs range up to $\sim 360\,km\,s^{-1}$ in NGC 6240 (Doyon et al. 1994) and have been measured successfully by Shier, Rieke & Rieke (1996) with a velocity resolution of $\sim 80\,km\,s^{-1}$.

AO imaging of NGC 3690 (Lai et al. 1999) has revealed the presence of at least six super star clusters with $K \sim 15.8$–$16.3\,mag$ and $V - K$ ranging from -0.4 to 1.4, which are unresolved at $0.2''$ resolution. It is unclear whether this emission is stellar or is due to ionised gas in giant H II regions. However, their existence is important because of the high specific frequency of globular clusters in giant elliptical galaxies, the possible ULIRG end-products. Globular clusters do seem to form during galaxy mergers (e.g. Schweiser & Seitzer 1998). Near-infrared spectroscopy with NIFS of super star clusters in objects like NGC 3690 will help define their nature and may provide indications of their metallicities. Measurements of their velocity dispersion relative to the main nuclei will provide information on the nuclear masses and the merger dynamics. A signal-to-noise ratio of ~ 36 per spectral pixel will be achieved with NIFS in the K band in $1800\,s$ with a $0.1'' \times 0.1''$ aperture on continuum objects with $K \sim 16\,mag$, similar to the NGC 3690 clusters.

There are no suitable OIWFS guide stars for either Arp 220 or NGC 1614 within the $120''$ diameter ALTAIR field of view. Suitable guide stars exist for NGC 6240, and the two nuclei in NGC 3690 can be used as guide objects for each other. The bright optical cores of these objects can be used as AO guide objects.

5.11 Dynamical Evolution of High-redshift Galaxies

Using Gemini with NIFS and ALTAIR, it may be possible to probe the properties of normal disk galaxies to redshifts $z \sim 1$. The internal kinematics of high-redshift galaxies are fundamentally related to the galaxy mass. Recent evidence suggests that the star formation rates in galaxies at $z \sim 1$ were up to an order of magnitude higher than in present-day galaxies (Madau et al. 1996; Glazebrook et al. 1999), from which it is inferred that disk galaxies have undergone substantial evolution during the intervening period. The Tully–Fisher relation expresses the relationship between rotational velocity and disk luminosity for present-day disk galaxies. If enhanced star formation in disk galaxies at $z \sim 1$ boosts their luminosities by a factor of ~ 10, the Tully–Fisher relation predicts that high-redshift galaxies will have rotational velocities lower by a factor of ~ 2 than present-day disk galaxies of similar luminosity. Measurement of disk-galaxy internal dynamics can therefore be used to trace the evolution in mass-to-light ratio of the underlying stellar population, and hence directly confront theories for the evolution of galaxies over cosmic time. Vogt et al. (1996, 1997) have measured rotation curves for 16 faint field galaxies with redshifts extending to $z \sim 1$

based on the [O II] $\lambda 3727$ emission line. These data demonstrate that at least some massive disk galaxies existed at $z \sim 1$. The rotational velocities for these high-luminosity galaxies indicate only a modest increase in luminosity of ~ 0.4 mag in M_B relative to the local Tully–Fisher relation. However, evidence is accumulating that the degree of luminosity evolution to $z \sim 1$ depends on galaxy mass (Koo et al. 1995; Rix et al. 1997; Simard & Pritchet 1998), with less massive, small disk galaxies undergoing larger evolution. Spatially and spectrally resolved observations of lower-mass galaxies are therefore of greatest importance; the bulk of the star formation since $z \sim 1$ may have occurred in these systems. Confirmation that high-redshift disk galaxies undergo ordered rotation is also needed, since this assumption underpins interpretations based on the Tully–Fisher relation.

Hα is the strongest emission line in the optical spectra of disk galaxies, it is the emission line most directly related to star formation rate, and it is less affected by dust extinction than [O II] $\lambda 3727$. At $z > 0.5$, Hα is redshifted into the near-infrared region that is accessible with NIFS. Glazebrook et al. (1999) have detected Hα in several $z \sim 1$ galaxies with a flux limit of $\sim 10^{-23}$ W cm^{-2}. At $z \sim 1$, Hα is redshifted to $1.3\,\mu$m, which is accessible with the NIFS J grating. Velocity resolutions of ~ 50 km s^{-1} are needed to adequately resolve the rotational velocity structure expected in small, low-mass disk galaxies at $z \sim 1$ (Koo et al. 1995). Spectral resolutions of this order are also required to adequately separate terrestrial OH airglow emission lines in the J band so that complete galaxy rotation curves can be recorded for significant samples of objects without contamination by OH emission lines. Spatially resolved spectroscopy, as opposed to integrated line profiles, is essential to allow confident interpretation of emission-line kinematics as being due to circular rotation of the galaxy disk.

Large disk galaxies at $z \sim 1$ typically have disk scale lengths $R_D < 6$ kpc (Schade et al. 1996; Simard et al. 1999), corresponding to $< 0.8''$ on the sky. However, high-redshift galaxies have been identified with disk scale lengths down to $R_D \sim 1$ kpc ($\sim 0.13''$; Schade et al. 1996; Simard et al. 1999), despite these galaxies having B-band luminosities comparable to those of present-day L^* galaxies. These high-surface-brightness, small objects are the strongly starbursting, low-mass galaxies that are likely to provide the best test of mass-dependent luminosity evolution (Broadhurst, Ellis & Shanks 1988). AO spatial resolution will be required for adequate measurement of rotation curves for these key objects. Galaxy rotation curves are characterised by solid-body rotation out to approximately R_D, and typically do not reach maximum velocity until $\sim 2 R_D$. It will be necessary to trace Hα emission-line profiles to $\sim 1.6''$ in the largest galaxies, and $\sim 0.25''$ in the smallest objects known. Due to relativistic effects, angular scales change little beyond $z \sim 1$ so the same requirements apply to higher-redshift galaxies.

About 25% of galaxies at $z \sim 0.3$ have [O II] kinematics unrelated to disk rotation, and have been classified as 'kinematically anomalous' (Simard & Pritchet 1998). NIFS will be well suited to studying the complex kinematics of these possible merger systems at high redshifts. If low-mass galaxies are the most actively star-forming galaxies at $z \sim 1$, they will be more susceptible to kinematic anomalies due to supernova-driven winds and nuclear outflows than their higher-mass counterparts, and will present a more diverse range of kinematics when studied with NIFS.

In addition to the above physical criteria, galaxies suitable for observation with NIFS must satisfy two further criteria: they must have redshifts that avoid the strong OH airglow lines in the J band, and they must have suitable AO and OIWFS guide stars. Only a limited number of candidates can be found in existing high-redshift galaxy samples. However, it should soon be possible to select samples of high-redshift galaxies near bright stars, using photometric redshift criteria and Sloan Digital Sky Survey data.

The performance of NIFS for these observations is affected by the lower Strehl ratio of only ~ 0.2 that will be achieved in the J band, and by the detector read noise and dark current, which will be significant relative to the sky background detected between OH airglow emission lines. Observations of Hα in high-redshift disk galaxies have been simulated by adopting the 'universal' disk galaxy rotation curve of Persic & Salucci (1991). The Hα luminosity in $z \sim 1$ galaxies is uncertain. The relation

$$M(B_{AB}) = 46.7 - 1.6 \log L(\text{H}\alpha) \qquad (2)$$

between the AB absolute blue magnitude, $M(B_{AB})$, and Hα luminosity in erg s^{-1}, $L(\text{H}\alpha)$, for $z < 0.3$ disk galaxies in the Canada–France redshift survey (Tresse & Maddox 1998) has been adopted, and the Hα emission is assumed to be distributed in an exponential disk with the same scale length as the continuum light. As a test case, we consider the $z = 0.9877$ Sc galaxy 064-4412, for which a rotation curve has been measured in redshifted [O II] $\lambda 3727$ using the Keck telescope (Vogt et al. 1996). This galaxy has a disk scale length of 4.1 kpc, an inclination of $68°$, B-band extinction $A_B = 0.61$ mag, absolute blue magnitude $M_B = -21.4$ mag, and a terminal rotational velocity of 265 ± 30 km s^{-1}. The Hα rotation curve at this particular redshift is contaminated by OH airglow lines, making it necessary to adopt a slightly different redshift of 0.996. A simulated raw 3600 s J-grating exposure of a galaxy with these parameters is shown in Figure 6. The signal-to-noise ratio in this raw image is insufficient to allow reliable measurement of a Hα rotation curve. The noise in the image is dominated by a fixed dark-current pattern expected to be present. If the dark current of the NIFS detector is sufficiently stable, it will be possible to remove this pattern, without adding further noise, by subtracting the median of several 1 hr dark exposures obtained during daytime. This requirement places tight constraints on the required stability of the detector dark current over periods of many hours. A dark-subtracted version of the Hα image is shown in Figure 7, assuming that the dark-current pattern can be
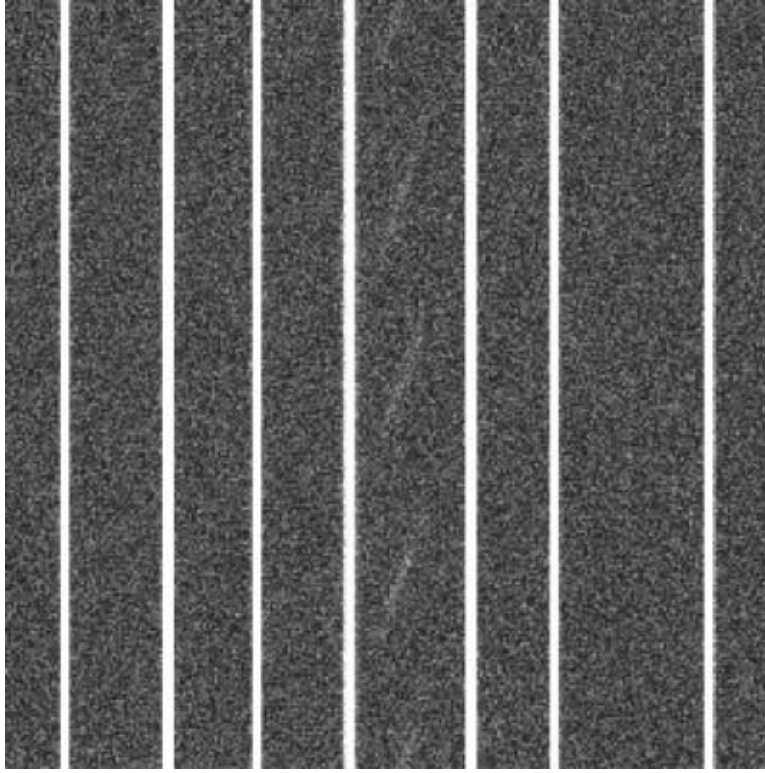
Figure 6 Central region of a simulated raw 3600 s *J*-grating exposure of Hα in a disk galaxy at $z = 0\cdot996$. The signal-to-noise ratio is limited by the fixed dark-current pattern.
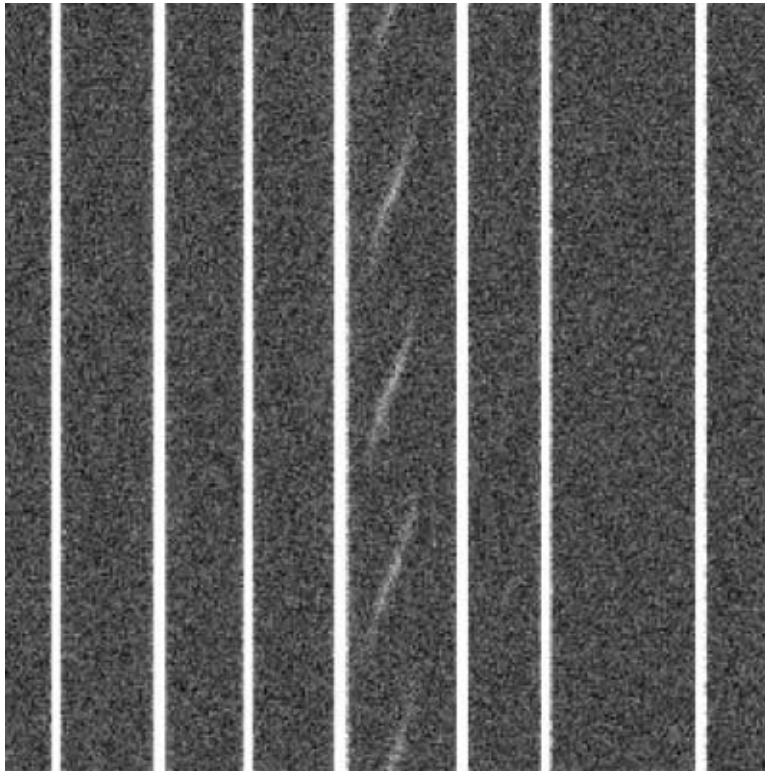

Figure 7 Dark-subtracted version of the $z = 0\cdot996$ disk galaxy Hα spectrum shown in Figure 6.

accurately removed. The Hα rotation curves for the central five slitlets are now seen more clearly and can probably be traced over nearly the full field of view using a maximum likelihood fitting technique (e.g. Simard & Pritchet 1999). No attempt has been made to subtract the OH airglow emission since this does not contaminate the Hα spectra in this simulation. This may be necessary in real data. We conclude that it should be possible to measure Hα rotation curves in $z \sim 1$ disk galaxies with NIFS, if the detector dark current is sufficiently stable, if scattered light from OH airglow emission lines is adequately controlled, and if the Hα fluxes in real galaxies are similar to those assumed.

5.12 Lyman-break Galaxies

Among the most significant legacies of the Hubble Space Telescope have been its observations of the Hubble Deep Field and the insights into the nature of galaxies at high redshift that have resulted from these observations. The high redshifts ($z > 3$) of many galaxies in the Hubble Deep Field can be deduced from their absence in ultraviolet images sampling the observed spectrum below the redshifted Lyman continuum absorption edge; radiation below the Lyman continuum edge is absorbed by intervening hydrogen clouds. These objects are known as 'Lyman-break' galaxies. They are among the most distant normal galaxies known.

Estimates of the star formation rates in Lyman-break galaxies are based on their rest-frame ultraviolet continuum luminosities. The global star formation rate at $z > 3$ is quite modest and suggests that we see these galaxies before the bulk of the star formation in the universe had taken place (Madau et al. 1996). This result is of immense significance for models of the formation and evolution of galaxies. However, the star formation rates on which it is based are questionable, due primarily to the unknown and potentially large effect of extinction by dust clouds within the galaxies on the measured rest-frame ultraviolet continuum fluxes. Many paths are currently being pursued to obtain more definitive star formation rates for these galaxies.

Hydrogen recombination lines provide the most direct measure of star formation rate, and in Lyman-break galaxies Hβ is redshifted into the K band. Measurement of the Hβ luminosities in Lyman-break galaxies will therefore provide far more direct estimates of the star formation rates for these galaxies. Observations of Hβ in Lyman-break galaxies have already been attempted with 4 m telescopes (Pettini et al. 1998). However, the signal-to-noise ratio obtained was barely sufficient to provide convincing detections of the line. Taken at face value, these results suggest star formation rates a factor between ~ 0.7 and ~ 7 larger than those deduced from ultraviolet continuum measurements. This result needs to be confirmed and extended using higher signal-to-noise ratio K-band spectra.

Nothing is known about the dynamics or masses of these distant, young galaxies. Moderate-resolution, near-infrared observations with NIFS of redshifted Hβ in Lyman-break galaxies have the potential to spatially resolve velocity structure in these galaxies that would indicate whether they are undergoing ordered rotation or still accumulating sub-galactic components and are yet to settle into a stable dynamical structure. Even crude velocity measurements would provide the first constraints on the masses of these galaxy building blocks.

Typical Hβ emission line fluxes for Lyman-break galaxies are a few times 10^{-24} W cm^{-2}. At a redshift of $z \sim 3.5$, Hβ is shifted to $2.19\,\mu$m in the K band. Pettini et al. (1998) used spectral resolving powers of 2000–2500 for their observations. Lyman-break galaxies are known to be small but resolved at AO resolution, with half light radii of $\sim 0.2''$–$0.3''$ (e.g. Steidel et al. 1996). Our ability to detect [O III] $\lambda 5007$ and Hβ at $z > 3.1$ with NIFS will depend on the degree to which this emission is clumped on scales matching the NIFS spatial resolution of $\sim 0.1''$. In fact, many young galaxies are composed of discrete, compact emission regions (e.g. Weedman et al. 1998), making them well suited to AO-corrected imaging spectroscopic observations with NIFS if the line fluxes are sufficiently high. If the Lyman-break galaxies detected by Pettini et al. (1998) are composed of ~ 5 clumps with sizes of $0.2'' \times 0.2''$, the typical emission-line surface brightness of each clump will be $\sim 5 \times 10^{-24}$ W cm^{-2} arcsec^{-2}. A 5σ detection of this feature averaged over $0.2'' \times 0.2''$ should be achieved in ~ 2 hr. Significantly higher signal-to-noise ratios would be required to measure dynamical information. High Strehl ratios will be required to reduce sky contamination and to measure velocity differences between individual clumps. Laser guide stars will most likely be needed for objects in the Hubble Deep Field. OIWFS guide stars may be problematic for these objects.

6 Context

The breadth of science possible with NIFS is critically dependent on how many interesting objects have both high enough surface brightness to measure and the necessary AOWFS and OIWFS guide stars. This issue is being actively pursued through the development of lists of actual observing targets. RSAA is continuing to develop the NIFS design and has already begun duplicating NIRI components for use in NIFS. The NIFS Critical Design Review is scheduled for February 2001, when the breadth of potential science and the final spectrograph design will be reviewed. Commissioning on Gemini North is currently scheduled for early 2003.

References

Ali, B., Carr, J. S., DePoy, D. L., Frogel, J. A., & Sellgren, K. 1995, AJ, 110, 2415

Axon, D. J., Marconi, A., Capetti, A., Macchetto, F. D., Schreier, E., & Robinson, A. 1998, ApJ, 496, L75

Bender, R., Kormendy, J., & Dehnen, W. 1996, ApJ, 464, L123

Blum, R. D., Damineli, A., & Conti, P. S. 1999, AJ, 117, 1392

Blum, R. D., Ramond, T. M., Conti, P. S., Figer, D. F., & Sellgren, K. 1997, AJ, 113, 1855

Blum, R. D., Sellgren, K., & DePoy, D. L. 1996, ApJ, 470, 864

Böker, T., van der Marel, R. P., & Vacca, W. D. 1999, AJ, 118, 831

Borne, K., Bushouse, H., Lucas, R. A., & Colina, L. 2000, ApJ, 529, L77

Bower, G. A., et al. 1998, ApJ, 492, L111

Broadhurst, T. J., Ellis, R. S., & Shanks, T. 1988, MNRAS, 235, 827

Buckle, J. V., Hatchell, J., & Fuller, G. A. 1999, A&A, 348, 584

Capetti, A., Axon, D. J., Macchetto, F. D., Sparks, W. B., & Boksenberg, A. 1996, ApJ, 469, 554

Chapman, S. C., Walker, G. A. H., & Morris, S. L. 1999, in Astronomy with Adaptive Optics: Present Results and Future Programs, ESO Conference and Workshop Proc., 56, ed. D. Bonaccini, (Garching: ESO), p.73

Cotera, A., Erickson, E. F., Colgan, S. W. J., Simpson, J. P., Allen, D. A., & Burton, M. 1996, ApJ, 461, 750

Davidge, T. J., Rigaut, F., Doyon, R., & Crampton, D. 1997a, AJ, 113, 2094

Davidge, T. J., Simons, D. A., Rigaut, F., Doyon, R., & Crampton, D. 1997b, AJ, 114, 2586

Doyon, R., Wells, M., Wright, G. S., Joseph, R. D., Nadeau, D., & James, P. A. 1994, ApJ, 437, L23

Eckart, A., & Genzel, R. 1996, Nature, 383, 415

Eckart, A., & Genzel, R. 1997, MNRAS, 284, 576

Eckart, A., Genzel, R., Hofmann, R., Sams, B. J., & Tacconi-Garman, L. E. 1995, ApJ, 445, L23

Ellerbroek, B. L., & Tyler, D. W. 1998, PASP, 110, 165

Faber, S. M., et al. 1997, AJ, 114, 1771

Ferland, G. J., & Netzer, H. 1983, ApJ, 264, 105

Ferrarese, L., Ford, H. C., & Jaffe, W. 1996, ApJ, 470, 440

Ford, H. C., Tsvetanov, Z. I., Ferrarese, L., & Jaffe, W. 1998, in The Central Regions of the Galaxy and Galaxies, IAU Symp. 184, ed. Y. Sofue (Dordrecht: Kluwer), 377

Frogel, J. A., Persson, S. E., & Cohen, J. G. 1981, ApJ, 246, 842

Gaffney, N. I., Lester, D. F., & Doppmann, G. 1995, PASP, 107, 68

Geballe, T. R., Kulkarni, S. R., Woodward, C. E., & Sloan, G. C. 1996, ApJ, 467, L101

Genzel, R., Eckart, A., Ott, T., & Eisenhauer, F. 1997, MNRAS, 291, 219

Ghez, A. M., Klein, B. L., Morris, M., & Becklin, E. E. 1998, ApJ, 509, 678

Glazebrook, K., Blake, C., Economou, F., Lilly, S., & Colless, M. 1999, MNRAS, 306, 843

Gordon, K. D., Hanson, M. M., Clayton, G. C., Rieke, G. H., & Misselt, K. A. 1999, ApJ, 519, 165

Hanson, M. M., Conti, P. S., & Rieke, M. J. 1996, ApJS, 107, 281

Hanson, M. M., Howarth, I. D., & Conti, P. S. 1997, ApJ, 489, 698

Hanson, M. M., Rieke, G. H., & Luhman, K. L. 1998, AJ, 116, 1915

Hartigan, P. 1989, ApJ, 339, 987

Ho, L. C., Filippenko, A. V., & Sargent, W. L. W. 1997, ApJ, 487, 568

Hodapp, K.-W., & Deane, J. 1993, ApJS, 88, 119

Koo, D. C., et al. 1995, ApJ, 440, L49

Kormendy, J., & McClure, R. D. 1993, AJ, 105, 1793

Kormendy, J., & Richstone, D. O. 1995, ARA&A, 33, 581

Kormendy, J., & Sanders, D. B. 1992, ApJ, 390, L53

Krist, J. E., et al. 1999, ApJ, 515, L35

Lada, E. A., DePoy, D. L., Evans, N. J., II, & Gatley, I. 1991, ApJ, 371, 171

Lai, O., Rouan, D., Rigaut, F., Doyon, R., & Lacombe, F. 1999, A&A, 351, 834

Larkin, J. E., Armus, L., Knop, R. A., Matthews, K., & Soifer, B. T. 1995, ApJ, 452, 599

Lauer, T. R., et al. 1993, AJ, 106, 1436

Lauer, T. R., et al. 1995, AJ, 110, 2622

Lauer, T. R., et al. 1996, ApJ, 471, L79

Leitherer, C., et al. 1999, ApJS, 123, 3

Luhman, K. L., & Rieke, G. H. 1998, ApJ, 497, 354

Madau, P., Ferguson, H. C., Dickinson, M. E., Giavalisco, M., Steidel, C. C., & Fruchter, A. 1996, MNRAS, 283, 1388

Maiolino, R., Krabbe, A., Thatte, N., & Genzel, R. 1998, ApJ, 493, 650

Marco, O., & Alloin, D. 1998, A&A, 336, 823

Marco, O., & Alloin, D. 2000, A&A, 353, 465

Marco, O., Alloin, D., & Beuzit, J. L. 1997, A&A, 320, 399

McGregor, P. J., Conroy, P., Bloxham, G., & van Harmelen, J. 1999, PASA, 16, 273

Norman, C., & Scoville, N. 1988, ApJ, 332, 124

Origlia, L., Ferraro, F. R., Fusi Pecci, F., & Oliva, E. 1997, A&A, 321, 859

Pedlar, A., Unger, S. W., & Dyson, J. E. 1985, MNRAS, 214, 463

Persic, M., & Salucci, P. 1991, ApJ, 368, 60

Pettini, M., Kellogg, M., Steidel, C. C., Dickinson, M., Adelberger, K. L., & Giavalisco, M. 1998, ApJ, 508, 539

Puxley, P. J., & Brand, P. W. J. L. 1999, ApJ, 514, 675

Racine, R., Walker, G. A. H., Nadeau, D., Doyon, R., & Marois, C. 1999, PASP, 111, 587

Ratnatunga, K. U., & Bahcall, J. N. 1985, ApJS, 59, 63

Rix, H.-W., Guhathakurta, P., Colless, M., & Ing, K. 1997, MNRAS, 285, 779

Rouan, D., et al. 1998, A&A, 339, 687

Sahai, R., et al. 1998, ApJ, 493, 301

Sahai, R., et al. 1999a, AJ, 118, 468

Sahai, R., te Lintel Hekkert, P., Morris, M., Zijlstra, A., & Likkel, L. 1999b, ApJ, 514, L115

Sahai, R., & Trauger, J. T. 1998, AJ, 116, 1357

Sakamoto, K., Scoville, N. Z., Yun, M. S., Crosas, M., Genzel, R., & Tacconi, L. J. 1999, ApJ, 514, 68

Sanders, D. B., et al. 1988, ApJ, 325, 74

Schade, D., Lilly, S. J., Le Fèvre, O., Hammer, F., & Crampton, D. 1996, ApJ, 464, 79

Schinnerer, E., Eckart, A., Quirrenbach, A., Böker, T., Tacconi-Garman, L. E., & Krabbe, A. 1997, ApJ, 488, 174

Schweiser, F., & Seitzer, P. 1998, AJ, 116, 2206

Scoville, N. Z., et al. 1998, ApJ, 492, L107

Shier, L. M., Rieke, M. J., & Rieke, G. H. 1996, ApJ, 470, 222

Simard, L., et al. 1999, ApJ, 519, 563

Simard, L., & Pritchet, C. J. 1998, ApJ, 505, 96

Simard, L., & Pritchet, C. J. 1999, PASP, 111, 453

Smith, M. D. 1995, A&A, 296, 789

Solomon, P. M., Downes, D., & Radford, S. J. E. 1992, ApJ, 387, L55

Solomon, P. M., Downes, D., Radford, S. J. E., & Barrett, J. W. 1997, ApJ, 478, 144

Steffen, W., Gomez, J. L., Raga, A. C., & Williams, R. J. R. 1997, ApJ, 491, 73

Steidel, C. C., Giavalisco, M., Dickinson, M., & Adelberger, K. L. 1996, AJ, 112, 352

Tacconi-Garman, L. E., Sternberg, A., & Eckart, A. 1996, AJ, 112, 918

Taylor, D., Dyson, J. E., & Axon, D. J. 1992, MNRAS, 255, 351

Terlevich, R., & Melnick, J. 1985, MNRAS, 213, 841

Thatte, N., Quirrenbach, A., Genzel, R., Maiolino, R., & Tecza, M. 1997, ApJ, 490, 238

Tremaine, S. 1995, AJ, 110, 628

Tresse, L., & Maddox, S. J. 1998 ApJ, 495, 691

van der Werf, P. P., et al. 1993, ApJ, 405, 522

Veilleux, S., Goodrich, R. W., & Hill, G. J. 1997, ApJ, 477, 631

Véran, J. P., Rigaut, F., Rouan, D., & Maître, H. 1997, JOSA A, 14(11)

Vogt, N. P., et al. 1996, ApJ, 465, L15

Vogt, N. P., et al. 1997, ApJ, 479, L121

Wandel, A., Peterson, B. M., & Malkan, M. A. 1999, ApJ, 526, 579

Weedman, D. W., Wolovitz, J. B., Bershady, M. A., & Schneider, D. P. 1998, AJ, 116, 1643

Wilson, A. S., & Tsvetanov, Z. I. 1994, AJ, 107, 1227

Winge, C., Axon, D. J., Macchetto, F. D., & Capetti, A. 1997, ApJ, 487, L121

Wright, G. S., James, P. A., Joseph, R. D., & McLean, I. S. 1990, Nature, 344, 417